LETTER

doi:10.1038/nature11932

Electrical image of passive mantle upwelling beneath the northern East Pacific Rise

Kerry Key[1], Steven Constable[1], Lijun Liu[2] & Anne Pommier[3]

Melt generated by mantle upwelling is fundamental to the production of new oceanic crust at mid-ocean ridges, yet the forces controlling this process are debated[1,2]. Passive-flow models predict symmetric upwelling due to viscous drag from the diverging tectonic plates, but have been challenged by geophysical observations of asymmetric upwelling[3–5] that suggest anomalous mantle pressure and temperature gradients[2,6,7], and by observations of concentrated upwelling centres[8] consistent with active models where buoyancy forces give rise to focused convective flow[2]. Here we use sea-floor magnetotelluric soundings at the fast-spreading northern East Pacific Rise to image mantle electrical structure to a depth of about 160 kilometres. Our data reveal a symmetric, high-conductivity region at depths of 20–90 kilometres that is consistent with partial melting of passively upwelling mantle[9–11]. The triangular region of conductive partial melt matches passive-flow predictions, suggesting that melt focusing to the ridge occurs in the porous melting region rather than along the shallower base of the thermal lithosphere. A deeper conductor observed east of the ridge at a depth of more than 100 kilometres is explained by asymmetric upwelling due to viscous coupling across two nearby transform faults. Significant electrical anisotropy occurs only in the shallowest mantle east of the ridge axis, where high vertical conductivity at depths of 10–20 kilometres indicates localized porous conduits. This suggests that a coincident seismic-velocity anomaly[12] is evidence of shallow magma transport channels[13,14] rather than deeper off-axis upwelling. We interpret the mantle electrical structure as evidence that plate-driven passive upwelling dominates this ridge segment, with dynamic forces being negligible.

We collected magnetotelluric data on the northern East Pacific Rise (EPR) to study the electrical structure of mantle upwelling, melt generation and magma transport to the crust at a mid-ocean ridge (Fig. 1). Magnetotelluric data record naturally occurring low-frequency electromagnetic variations that sense electrical conductivity, a physical property that primarily depends on temperature, mineralogy and the presence of fluids and their interconnectedness[10,11]. The upwelling region beneath mid-ocean ridges is a particularly suitable target for magnetotelluric exploration, because small fractions of conductive partial melt can greatly increase bulk conductivity from the generally low conductivity of unmelted peridotite[5,10,11,15].

The fast spreading EPR separates the Pacific and Cocos plates, which diverge symmetrically to produce new sea floor at a half-spreading rate of 55 km Myr^{-1}, while the entire ridge system migrates to the northwest at 50 km Myr^{-1} relative to a hotspot reference frame[16] (Fig. 1). The 8–11° N EPR ridge segment became a locus of scientific investigation after the first direct observations of extensive sea-floor volcanism[17]. Vigorous hydrothermal venting[18] and a continuous crustal magma chamber[19] suggest this ridge segment taps a robust mantle melt supply, a notion reinforced by a sea-floor eruption that buried several actively recording seismometers[20]. Seismic tomography shows the shallowest mantle at 9 km depth contains a low P-wave-velocity zone that follows the ridge crest along most of this segment, but which deviates 5–10 km east of the ridge near our magnetotelluric profile (Fig. 1), suggesting that melt delivery to the base of the crust is locally focused eastward here[12]. Despite a multitude of studies at this ridge segment, the deeper mantle upwelling region remained unexplored by a large geophysical array until this magnetotelluric study.

Our survey relied on broadband magnetotelluric instrumentation that is sensitive to the high frequencies required to constrain the shallow mantle[15] and that requires only 10–20 days of recording time, making array surveys possible with a single research cruise. The 200-km profile of 29 magnetotelluric stations contains a broad aperture suitable for imaging mantle upwelling but also has closely spaced stations near the ridge axis to constrain melt focusing to the base of the crust (Fig. 1). For comparison, the earlier MELT experiment obtained sensitivity to deeper upwelling structure using year-long deployments of 19 long-period instruments along a more sparely sampled 400-km transect[5]. We used regularized nonlinear data inversion to produce a smooth image of two-dimensional electrical resistivity constrained to about 160 km depth and to 100 km distance from the ridge axis (Fig. 2).

The inversion model reveals a prominent conductive region ($<100\,\Omega$ m resistivity) centred beneath the ridge axis. Conductivity (the reciprocal of resistivity) is greatest at depths of about 20–90 km and is largely symmetric about the ridge axis. The top of the conductive region displays a broad triangular shape that deepens away from the ridge, reaching depths of about 80–100 km at 100 km distance. Above the sides of this conductor, the mantle becomes significantly more resistive (100–2,000 Ω m). The deeper mantle, at depths >100 km, is less resistive than 60 Ω m, but is asymmetric with resistivity as low as 10 Ω m to the east. Model perturbation tests show that the central and deeper conductive regions are required to obtain a good fit to the data (see Supplementary Figs 7 and 8), although the deeper conductor is less well constrained owing to its location near the edge of the magnetotelluric array and its depth. Anisotropy is insignificant throughout most of the model, except beneath the ridge at 10–20 km depth and 0–10 km position, where conductivity is greatest in the vertical direction (Supplementary Fig. 5).

These conductive regions indicate that the upwelling mantle is undergoing significant partial melting. Mineral physics studies find that upwelling will trigger decompression melting of dry peridotite at a depth of about 65 km, where the ridge adiabat crosses the peridotite solidus[9]. However, the deeper extent of our conductive region agrees with experimental studies of mid-ocean-ridge basalt samples that show the upper-mantle source region is slightly damp, with 50–200 parts per million (p.p.m.) H_2O (refs 21, 22), resulting in a deeper peridotite solidus that promotes melting to around 100 km depth[9], depending on the amount of H_2O present. The presence of dissolved CO_2 has also been reported in mid-ocean-ridge contexts, and is thought to stabilize carbonated silicate partial melts at even greater depths[23,24], and the combination of CO_2 and H_2O may further enhance deep silicate melting[25].

Recent laboratory electrical conductivity studies have shown that small amounts of dissolved H_2O and CO_2 will increase the conductivity

[1]Institute of Geophysics and Planetary Physics, Scripps Institution of Oceanography, University of California, San Diego, La Jolla, California 92093, USA. [2]Department of Geology, College of Liberal Arts and Sciences, University of Illinois, Urbana, Illinois 61801, USA. [3]School of Earth and Space Exploration, Arizona State University, Tempe, Arizona 85287, USA.

of mantle partial melt[10,11]. Because these volatiles are preferentially partitioned into melt, the earliest deep melts will be the most conductive, whereas later shallower melts will have lower volatile fractions and hence display a conductivity that is transitional between the volatile-influenced and dry endmembers[11]. The low resistivity of 1–10 Ω m in the main conductive body is consistent with up to a few volume per cent partial melt, but the highly conductive core of the anomaly (0.3 Ω m) requires a significantly higher melt fraction (>10 vol.%)[10,11]. However, we warn against over-interpreting this high conductivity, because magnetotelluric data are primarily sensitive to the integrated conductance of conductive bodies; the inversion may be trading-off a narrow size for this core region with a compensating higher conductivity.

Because carbonate melts are much more conductive than silicate melt[11], the 10–60 Ω m resistivity beneath 100 km depth can be explained by a much lower amount of carbonate partial melt (<0.5 vol.%) that is stable at this depth. The moderately resistive gap separating the two conductive regions at around 100 km depth is intriguing, because the deeper carbonate melts should be migrating upward and enhancing conductivity there. However, experimental results have shown that when both silicate and carbonate melts are present, the solid matrix is preferentially wetted by silicate melt, and therefore carbonate would not necessarily be well connected[26]; it may also be diluted by the less conductive silicate melt[11]. We suggest that this gap represents the depth where silicate melt begins to dominate over carbonate melt, leading to an overall lower conductivity.

The melting region at depths shallower than 100 km in our study is unusually symmetric compared to geophysical observations at other mid-ocean ridges[1,4,8], but is juxtaposed with deeper asymmetric melting below 100 km. Although viscous drag from symmetrically diverging tectonic plates is thought to be the main driving force in mantle upwelling, asymmetric observations have required additional mechanisms in order to generate melt unevenly across the ridge. A strong westward asymmetry observed at the southern EPR was conjectured to arise from mantle pressure or temperature gradients[6,7]. Localized centres of upwelling observed in the Gulf of California do not align with the heavily segmented ridge axis, suggesting that melt may be dynamically concentrated through buoyant convective flow[8].

We carried out a three-dimensional flow simulation to study whether the deep asymmetry in our model could be explained solely by passive flow, or requires the addition of dynamic forces or lateral temperature and pressure gradients. Absolute plate motions were imposed as a boundary condition on a simulation domain that included both the Clipperton and Siqueiros transform offsets. Figure 3 shows the vertical velocity component of flow induced by the plate motions. In the upwelling mantle, melting occurs in proportion to the vertical velocity due to decompression but also depends on composition and adiabatic temperature. Because the melting rate for hydrous, carbonated peridotite is poorly known, we use vertical velocity as a proxy indicator for where deep incipient melts could be generated.

The deep upwelling shows an asymmetry between the transform offsets, with vertical velocities of 0.5–2.5 cm yr^{-1} biased to the east of the ridge axis at 100–250 km depth. Although we included westward ridge migration in the simulation via the absolute plate motions, it does not generate a significant asymmetry in melt production because migration only superimposes a horizontal shear to the deep flow[6,7]. This is further supported by the lack of asymmetry in the simulation far north of the Clipperton transform and far south of the Siqueiros transform. Rather, the deep asymmetry arises from viscous coupling across the transform offsets, which is intensified because both offsets jump to the east and are in relatively close proximity. This upwelling asymmetry will generate more melt to the east, offering an explanation for our observed asymmetry. However, our model contains deep carbonate melts extending much further off-axis than the peak in upwelling. Because the magnetotelluric inversion is imaging the amount of partial melt present rather than the melting rate implied by the vertical

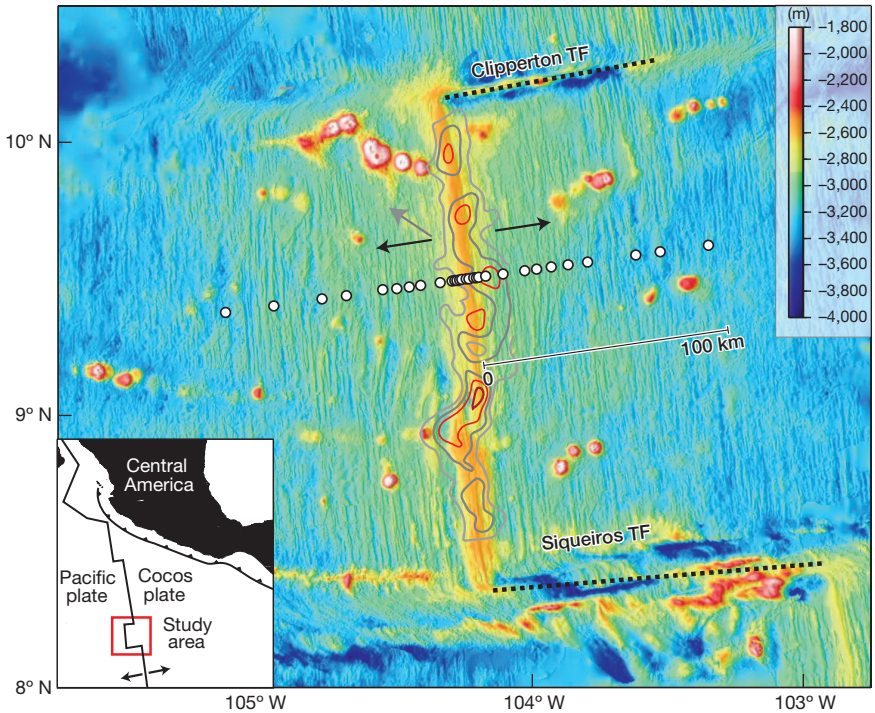

Figure 1 | Location of the magnetotelluric survey across the fast spreading East Pacific Rise. Twenty-nine sea-floor magnetotelluric stations (white circles) were deployed across the ridge axis at 9° 30′ N, about 1,000 km southwest of Central America (inset; study area boxed in red). The Pacific and Cocos plates diverge symmetrically (black arrows) while the entire ridge system migrates to the northwest relative to a fixed hotspot reference frame[16] (grey arrow). The Clipperton and Siqueiros transform faults (TF) bound this ridge segment to the north and south. Slow seismic P-wave velocity contours (velocities <7.6 km s^{-1}) found by seismic tomography of the uppermost few kilometres of mantle[12] follow the ridge crest along most of the segment, but deviate to the east near the magnetotelluric profile. The colour scale shows sea-floor topography and the 100-km scale bar indicates the half-aperture of the magnetotelluric array.

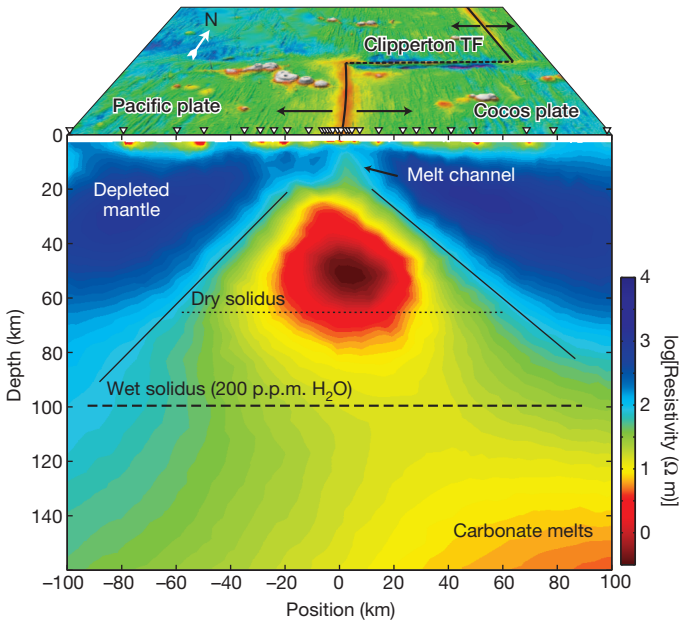

Figure 2 | Magnetotelluric resistivity image of mantle upwelling beneath the East Pacific Rise. Top, surface view of sea-floor topography. Main panel, colours show log[resistivity (Ω m)] in the vertical direction obtained from nonlinear inversion of data from the sea-floor magnetotelluric stations (inverted triangles in surface view). Green to red colours indicate high conductivity (low resistivity) due to partial melts generated in the upwelling mantle. The full anisotropic resistivity results are shown in Supplementary Fig. 5. Solidus depths for dry and wet peridotite[9] are shown as horizontal lines.

velocity, it is possible that this conductor represents melt that has ascended from greater depths; if deep off-axis melt is partially entrained in the mantle flow, it may be transported further to the east of the ridge axis owing to the westward ridge migration.

Upwelling at depths shallower than 100 km is intensive and symmetric beneath the ridge axis, in agreement with the prominent zone of silicate melt indicated by the high conductivity in our model (Fig. 3b). Despite the smoothing penalty applied during the data inversion, our model shows a rapid resistivity increase that coincides with the sloping boundaries of the upwelling mantle. Along this boundary, the flow pattern turns from upwelling to horizontal flow as the mantle begins to be dragged off-axis. Because the high resistivity agrees with that of melt-free dry olivine[27], this transition away from the inferred melting region is consistent with the closure or compaction of the porous melt network generated by upwelling. This implies that buoyant melt is focused to the ridge axis by the shape of the porous melting region, rather than by upward migration to the base of the much shallower thermal lithosphere defined by the half-space cooling model (Fig. 3b).

The shallow uppermost mantle above 20 km depth is predominantly resistive, suggesting it is largely unmolten with a negligible porosity. However, moderately low vertical resistivity spanning from the ridge axis to 10 km to the east is consistent with a vertical melt channel connecting from the deeper melting region to the base of the crust (Fig. 2). This feature occurs where seismic tomography found a low-velocity anomaly directly beneath the crust[12]. Our model suggests that the off-axis velocity anomaly is due to a shallow melt transport channel or network of channels[13] rather than reflecting deeper upwelling asymmetry. Highly porous transport channels could allow for rapid magma ascent to the crust[13]. This may explain why the high conductivity imaged at depths >20 km does not extend all the way to the base of the crust beneath the ridge axis. Magma generated in the upwelling mantle may reach a critical depth near the top of the melting region where it is efficiently transported to the crust through porous channels that arise episodically in space and time.

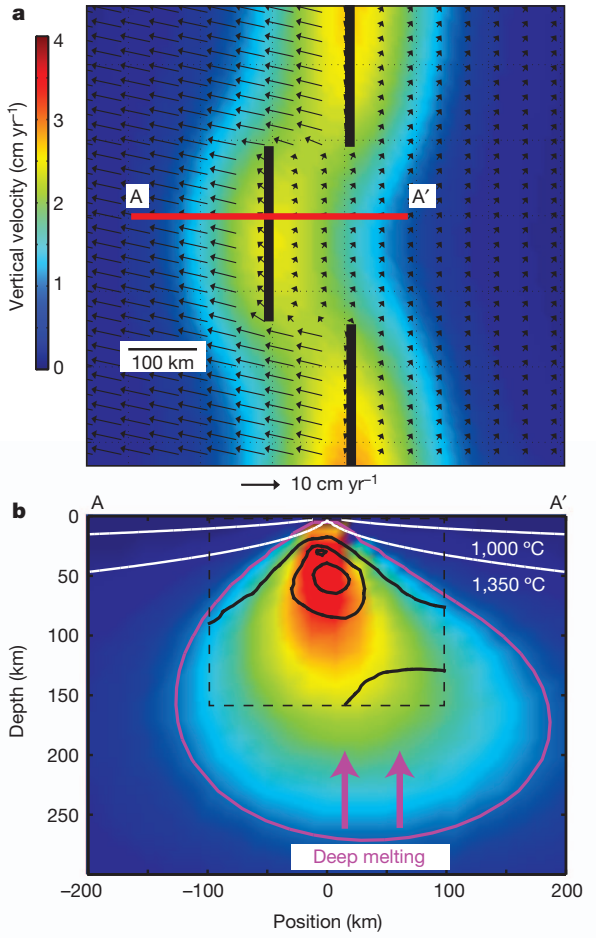

Figure 3 | Three-dimensional passive-flow simulation of the EPR kinematics, including ridge migration, sea-floor spreading and the Clipperton and Siqueiros transform offsets. **a**, Map view showing the imposed absolute plate motions of the Pacific and Cocos plates (black arrows) and the simulated upwelling vertical velocity at 150 km depth (shaded colours). **b**, Cross-section of vertical velocity along profile A–A′ (in **a**), which crosses the ridge axis at the same position as the magnetotelluric profile. The magenta line contours 1 cm yr^{-1} vertical velocity, highlighting the deep asymmetry to the east (right). Black lines delineate 0.1, 1 and 10 Ω m resistivity contours from the magnetotelluric inversion model (Fig. 2). White lines show isotherms for a half-space cooling model.

METHODS SUMMARY

We used a robust array processing method[28] to estimate magnetotelluric responses from the raw time series and inverted the responses for triaxially anisotropic conductivity using nonlinear two-dimensional inversion implemented with an adaptive finite element algorithm[29,30]. Flow modelling of mantle upwelling due to absolute plate motions was accomplished using a finite element approach.

Full Methods and any associated references are available in the online version of the paper.

Received 16 October 2012; accepted 23 January 2013.

1. Forsyth, D. W. *et al.* Imaging the deep seismic structure beneath a mid-ocean ridge; the MELT experiment. *Science* **280,** 1221–1224 (1998).
2. Katz, R. F. Porosity-driven convection and asymmetry beneath mid-ocean ridges. *Geochem. Geophys. Geosyst.* **11,** Q0AC07 (2010).
3. Hammond, W. C. & Toomey, D. R. Seismic velocity anisotropy and heterogeneity beneath the Mantle Electromagnetic and Tomography Experiment (MELT) region of the East Pacific Rise from analysis of P and S body waves. *J. Geophys. Res.* **108,** 2176, http://dx.doi.org/10.1029/2002JB001789 (2003).
4. Dunn, R. A. & Forsyth, D. W. Imaging the transition between the region of mantle melt generation and the crustal magma chamber beneath the southern East Pacific Rise with short-period Love waves. *J. Geophys. Res.* **108,** 2352, http://dx.doi.org/10.1029/2002JB002217 (2003).

5. Baba, K., Chave, A. D., Evans, R. L., Hirth, G. & Mackie, R. L. Mantle dynamics beneath the East Pacific Rise at 17°S: insights from the Mantle Electromagnetic and Tomography (MELT) experiment. *J. Geophys. Res.* **111,** B02101, http://dx.doi.org/10.1029/2004JB003598 (2006).
6. Conder, J. A., Forsyth, D. W. & Parmentier, E. M. Asthenospheric flow and asymmetry of the East Pacific Rise, MELT area. *J. Geophys. Res.* **107,** 2344, http://dx.doi.org/10.1029/2001JB000807 (2002).
7. Toomey, D. R. *et al.* Asymmetric mantle dynamics in the MELT region of the East Pacific Rise. *Earth Planet. Sci. Lett.* **200,** 287–295 (2002).
8. Wang, Y., Forsyth, D. W. & Savage, B. Convective upwelling in the mantle beneath the Gulf of California. *Nature* **462,** 499–501 (2009).
9. Hirschmann, M. M., Tenner, T., Aubaud, C. & Withers, A. C. Dehydration melting of nominally anhydrous mantle: the primacy of partitioning. *Phys. Earth Planet. Inter.* **176,** 54–68 (2009).
10. Ni, H., Keppler, H. & Behrens, H. Electrical conductivity of hydrous basaltic melts: implications for partial melting in the upper mantle. *Contrib. Mineral. Petrol.* **162,** 637–650 (2011).
11. Yoshino, T., Mclsaac, E., Laumonier, M. & Katsura, T. Electrical conductivity of partial molten carbonate peridotite. *Phys. Earth Planet. Inter.* **194–195,** 1–9 (2012).
12. Toomey, D. R., Jousselin, D., Dunn, R. A., Wilcock, W. S. D. & Detrick, R. S. Skew of mantle upwelling beneath the East Pacific Rise governs segmentation. *Nature* **446,** 409–414 (2007).
13. Katz, R. F. & Weatherley, S. M. Consequences of mantle heterogeneity for melt extraction at mid-ocean ridges. *Earth Planet. Sci Lett.* **335–336,** 226–237 (2012).
14. Aharonov, E., Whitehead, J. A., Kelemen, P. B. & Spiegelman, M. Channeling instability of upwelling melt in the mantle. *J. Geophys. Res.* **100** (B10), 20433–20450 (1995).
15. Key, K. & Constable, S. Broadband marine MT exploration of the East Pacific Rise at 9°50′N. *Geophys. Res. Lett.* **29**, 2054, http://dx.doi.org/10.1029/2002GL016035 (2002).
16. Gripp, A. E. & Gordon, R. G. Young tracks of hotspots and current plate velocities. *Geophys. J. Int.* **150,** 321–361 (2002).
17. Haymon, R. M. *et al.* Volcanic eruption of the mid-ocean ridge along the East Pacific Rise crest at 9°45–52′N: direct submersible observations of seafloor phenomena associated with an eruption event in April 1991. *Earth Planet. Sci. Lett.* **119,** 85–101 (1993).
18. Baker, E. T. *et al.* Hydrothermal plumes along the East Pacific Rise, 8°40′ to 11°50′N: plume distribution and relationship to the apparent magmatic budget. *Earth Planet. Sci. Lett.* **128,** 1–17 (1994).
19. Kent, G. M., Harding, A. J. & Orcutt, J. A. Distribution of magma beneath the East Pacific Rise between the Clipperton Transform and the 9°17′N Deval from forward modeling of common depth point data. *J. Geophys. Res. B* **98,** 13945–13969 (1993).
20. Tolstoy, M. *et al.* A seafloor spreading event captured by seismometers. *Science* **314,** 1920–1922 (2006).
21. Danyushevsky, L. V., Eggins, S. M., Falloon, T. J. & Christie, D. M. H_2O abundance in depleted to moderately enriched mid-ocean ridge magmas; part I: incompatible behaviour, implications for mantle storage, and origin of regional variations. *J. Petrol.* **41,** 1329–1364 (2000).
22. Saal, A. E., Hauri, E. H., Langmuir, C. H. & Perfit, M. R. Vapour undersaturation in primitive mid-ocean-ridge basalt and the volatile content of Earth's upper mantle. *Nature* **419,** 451–455 (2002).
23. Hirose, K. Partial melt compositions of carbonated peridotite at 3 GPa and role of CO_2 in alkali-basalt magma generation. *Geophys. Res. Lett.* **24,** 2837–2840 (1997).
24. Wendlandt, R. F. & Mysen, B. O. Melting phase relations of natural peridotite + CO_2 as a function of degree of partial melting at 15 and 30 kbar. *Am. Mineral.* **65,** 37–44 (1980).
25. Dasgupta, R., Hirschmann, M. M. & Smith, N. D. Water follows carbon: CO_2 incites deep silicate melting and dehydration beneath mid-ocean ridges. *Geology* **35,** 135–138 (2007).
26. Minarik, W. G. Complications to carbonate melt mobility due to the presence of an immiscible silicate melt. *J. Petrol.* **39,** 1965–1973 (1998).
27. Constable, S. SEO3: A new model of olivine electrical conductivity. *Geophys. J. Int.* **166,** 435–437 (2006).
28. Egbert, G. D. Robust multiple-station magnetotelluric data processing. *Geophys. J. Int.* **130,** 475–496 (1997).
29. Key, K. & Ovall, J. A parallel goal-oriented adaptive finite element method for 2.5-D electromagnetic modelling. *Geophys. J. Int.* **186,** 137–154 (2011).
30. Constable, S. C., Parker, R. L. & Constable, C. G. Occam's inversion — a practical algorithm for generating smooth models from electromagnetic sounding data. *Geophysics* **52,** 289–300 (1987).

Supplementary Information is available in the online version of the paper.

Acknowledgements We thank the captain and crew of R/V *Roger Revelle*, members of the scientific party (J. Behrens, G. Boran, G. Heinson, J. King, A. Massarweh, L. Terzi and C. Weiss), and the technical team (C. Armerding, P. Cheng, C. Berger, G. Englehorn, G. Howe, K. Callaway and J. Lemire). We thank D. Myer for assistance with the data processing and R. Katz for reviewing the manuscript. This work was funded by US NSF award OCE-0241597 and the Seafloor Electromagnetic Methods Consortium at Scripps Institution of Oceanography.

Author Contributions K.K. and S.C. collected and analysed the field data. A.P. and K.K. performed the melt calculations. L.L. carried out the mantle flow simulations. K.K. wrote most of the manuscript. All authors discussed the results and commented on the manuscript.

Author Information Reprints and permissions information is available at www.nature.com/reprints. The authors declare no competing financial interests. Readers are welcome to comment on the online version of the paper. Correspondence and requests for materials should be addressed to K.K. (kkey@ucsd.edu).

METHODS

Magnetotelluric data analysis. The 29 broadband magnetotelluric stations were deployed during a single month-long cruise, yielding frequency domain magnetotelluric responses in the 20–5,000 s period band. The station names are given in Supplementary Fig. 1 and the magnetotelluric data are shown in Supplementary Figs 2 and 3. Magnetotelluric impedance skews[31] for each station are displayed in Supplementary Fig. 4. Low skews from the ridge axis to the west are consistent with a predominantly two-dimensional conductivity beneath the ridge. Many stations on the Cocos plate have large impedance skews at periods of 100–1,000 s, indicating three-dimensional conductivity effects. These large skews are probably due to the 85 km lateral offset of ridge axis, and by inference the conductive upwelling region, across the Clipperton transform, which is located only 75 km north of the magnetotelluric profile. For our two-dimensional analysis, we omitted all transverse-electric (TE) data (that is, ridge-parallel electric fields) from sites s48 to s60 and only included transverse magnetic (TM) data (that is, ridge-perpendicular vertical current loops), because TM data are considered more reliable for two-dimensional interpretation in the presence of three-dimensional effects[31,32].

Nonlinear anisotropic inversion. We modelled the data using a regularized nonlinear inversion that solved for anisotropic electrical resistivity with a triaxial form:

$$\rho = \begin{bmatrix} \rho_x & 0 & 0 \\ 0 & \rho_y & 0 \\ 0 & 0 & \rho_z \end{bmatrix} \quad (1)$$

where the x direction is aligned with the ridge axis, y is ridge perpendicular and z points down. The inversion solved for the three unknown resistivity tensor elements on a grid of 7,728 triangular cells spanning from the sea floor into the mantle, with small cells conforming to the rugged sea-floor bathymetry and larger cells at depth. The total number of unknown parameters was 23,184.

The inversion follows the usual Occam's approach by minimizing the following functional[30]:

$$U = \|\partial m\|^2 + \mu^{-1}\|W(d - F(m))\|^2 \quad (2)$$

The first term measures the model roughness. The second term measures the fit of the model m ($\log_{10}$ resistivity) to the observed data d, weighted by the inverse data standard errors in the diagonal matrix W, where F is the forward modelling operator and $||...||$ is the two-norm. Occam uses an automatic search method to find the largest trade-off parameter μ that fits the data, thereby seeking the smoothest model fitting the data. For the triaxially anisotropic resistivity considered here, the model roughness term is expanded into the form:

$$\|\partial m\|^2 = \|\partial m_x\|^2 + \|\partial m_y\|^2 + \|\partial m_z\|^2 + \|m_x - m_y\|^2 + \|m_y - m_z\|^2 + \|m_z - m_x\|^2 \quad (3)$$

The first three terms measure the spatial roughness of each anisotropic resistivity component by differencing the values for adjacent resistivity parameters. The last three terms measure the degree of anisotropy within each cell so that the inversion only generates anisotropy where it is required to fit the observed data. Equation (3) has an implicit weighting of unity between the spatial roughness and anisotropic roughness measures so that neither is given preferential treatment by the inversion.

We applied a 10% error floor to the data and then ran the inversion until it found a minimum root-mean-squared (r.m.s.) misfit of 1.73. We then restarted the inversion and ran it to a target r.m.s. misfit that was 10% larger (1.90), to ensure the data were not being over-fitted. The inversion was started from a uniform 10 Ω m model. Supplementary Fig. 5 shows the resulting anisotropic inversion model and Supplementary Fig. 3 shows the corresponding model fits to the data.

We also carried out an inversion of only the TM mode data to examine differences in the inverted model structure as a function of data constraints (Supplementary Fig. 6). This inversion finds a deep asymmetric conductor below 100 km depth that is similar to the previous inversion of both the low-skew TE mode data and all TM data (Supplementary Fig. 5). The TM-only inversion similarly finds a shallower ridge-centred melting region, but its conductivity is much lower than the previous inversion that included TE data. This is not surprising because the TM mode is known to be less sensitive to the conductivity of two-dimensional conductors than the TE mode, but is more sensitive to the lateral edges of conductors than the TE mode[31].

Model sensitivity studies. We tested the sensitivity of the data to both the shallow (A) and deep (B) conductors and the sub-crustal vertical conductor (C) by erasing each feature and computing the corresponding change in data fit. Supplementary Fig. 7 shows the outline of these conductive regions, where the resistivity was increased to 100 Ω m (A and B) and 200 Ω m (C). Supplementary Fig. 8 shows the increase in the r.m.s. data misfit for each test. Removing the shallow conductor A resulted in an r.m.s. increase of 400% for the TE data and 20% for the TM data, showing that it is strongly required by the data. Removing the deeper conductor B resulted in a change of only 20% in the TM mode data fit, showing that it is less well constrained by the data, yet still required to obtain a good overall fit. Removing the vertical conductor C resulted in a 3% change in the TM mode fit; while this is a small change, individual sites have up to 9% worse data misfits when the conductor is removed, suggesting it is a necessary feature of the model.

Three-dimensional passive-flow modelling. We constructed a three-dimensional flow model simulating the kinematics of the EPR transform faults near 8° and 10° N using a finite element method[33]. The model domain spans 12° (latitude), 24° (longitude) and 1,000 km (depth), where the long enough east–west dimension of the box avoids the edge effects. A high mesh resolution (~7 km) was selected so that the flow pattern does not depend on the grid size. Plate motions were imposed as surface velocity boundary conditions, with a full spreading rate of 11 cm yr^{-1} and a northwestward ridge migration rate of 5 cm yr^{-1}, according to NUVEL1A[16]. Sea-floor ages were used to prescribe the upper thermal boundary layer, with zero age at the spreading centre, which increases to 30 Myr towards the edges of the box. A temperature- and depth-dependent viscosity structure was used, with the mean viscosities at depths of lithosphere, upper mantle, transition zone and lower mantle corresponding to 100, 0.01, 1, 30 (relative to 10^{21} Pa s), respectively.

31. Berdichevsky, M. & Dmitriev, V. I. *Models and Methods of Magnetotellurics* (Springer, 2008).
32. Wannamaker, P. E., Hohmann, G. W. & Ward, S. H. Magnetotelluric responses of three-dimensional bodies in layered earths. *Geophysics* **49,** 1517–1533 (1984).
33. Zhong, S., Zuber, M. T., Moresi, L. & Gurnis, M. Role of temperature-dependent viscosity and surface plates in spherical shell models of mantle convection. *J. Geophys. Res.* **105,** 11063–11082 (2000).